

Linear Theory of the Rayleigh–Taylor Instability at a Discontinuous Surface of a Relativistic Flow

Jin Matsumoto^{1*}, Miguel A. Aloy² and Manel Perucho^{2,3}

¹*Astrophysical Big Bang Laboratory, Riken, Wako, 351-0198, Japan*

²*Departament d’Astronomia i Astrofísica, Universitat de València, C/ Dr. Moliner, 50, 46100, Burjassot, València, Spain.*

³*Observatori Astronòmic, Universitat de València, C/ Catedràtic José Beltrán 2, 46980, Paterna, València, Spain.*

Accepted xxx, Received yyy, in original form zzz

ABSTRACT

We address the linear stability of a discontinuous surface of a relativistic flow in the context of a jet that oscillates radially as it propagates. The restoring force of the oscillation is expected to drive a Rayleigh–Taylor instability (RTI) at the interface between the jet and its cocoon. We perform a linear analysis and numerical simulations of the growth of the RTI in the transverse plane to the jet flow with a uniform acceleration. In this system, an inertia force due to the uniform acceleration acts as the restoring force for the oscillation. We find that not only the difference in the inertia between the two fluids separated by the interface but also the pressure at the interface helps to drive the RTI because of a difference in the Lorentz factor across the discontinuous surface of the jet. The dispersion relation indicates that the linear growth rate of each mode becomes maximum when the Lorentz factor of the jet is much larger than that of the cocoon and the pressure at the jet interface is relativistic. By comparing the linear growth rates of the RTI in the analytical model and the numerical simulations, the validity of our analytically derived dispersion relation for the relativistic RTI is confirmed.

Key words: galaxies: jets — instabilities — methods: analytical — methods: numerical — relativistic processes

1 INTRODUCTION

The interface between two fluids of different densities is unstable if the heavier fluid is supported above the lighter one against gravity, or equivalently if the lighter fluid accelerates the heavier one. This instability is known as the Rayleigh–Taylor instability (RTI, Rayleigh 1900; Taylor 1950). It is a fundamental process in hydrodynamics and plays an important role in many astrophysical contexts.

In massive stars, the composition interfaces between the hydrogen- and helium-rich layers and between the helium-rich layer and C+O core are Rayleigh–Taylor (RT) unstable after a supernova shock wave passes through them (Chevalier 1976; Ebisuzaki et al. 1989; Hachisu et al. 1992; Ono et al. 2013; Mao et al. 2015). The growth of such RTIs is thought to be a promising mechanism for the material mixing or the penetration of lighter and heavier elements into the neighboring layers in supernova explosions (Kifonidis et al. 2003; Wongwathanarat et al. 2015).

In addition to the above, the possibility of RTIs in supernova remnants has been discussed. The ejected stellar envelope associated with a supernova explosion is decelerated by the swept-up interstellar medium. The interface separating the denser ejecta from

the shocked interstellar medium is also RT unstable (Ferrand et al. 2012; Warren & Blondin 2013; Obergaulinger et al. 2014a). The growth of RTIs is responsible for the finger-like structures found in supernovae remnants. The stretching of the magnetic field lines by these RT fingers may help to amplify the magnetic field, thereby explaining the observed synchrotron emission from the thin shell of the supernova remnant (Jun et al. 1995; Jun & Norman 1996; Guo et al. 2012; Obergaulinger et al. 2014b).

The magnetic RTI (Hillier 2016) itself is also expected to be important for the emergence of magnetic flux from the solar interior (Isobe et al. 2005, 2006) and the buoyancy of bubbles in the solar prominence (Hillier et al. 2011, 2012). The magnetic tension suppresses the short-wavelength modes along the magnetic field except when the wavevector is perpendicular to the magnetic field. As a result of the different development of the magnetic RTI along and across the magnetic field lines, there is a preferential formation of astrophysical features elongated in the direction of the magnetic field.

In a super-Eddington outflow from an accretion disk, in which the outward acceleration due to the radiation force is larger than the inward gravitational pull of the central black hole, the radiation force drives RTIs. These instabilities are located at the photosphere of the accretion disk, since the density decreases outwardly there (Takeuchi et al. 2013, 2014). The radiation force acts as an external inertia force in the driving mechanism of this instability. The

* E-mail: jin.matsumoto@riken.jp

growth of radiation-driven RTIs may be responsible for the formation of clumpy structures in super-Eddington outflows.

The relativistic RTI is a key process in the dynamics of high-energy astrophysics. The contact discontinuity in a relativistic shell propagating through the interstellar medium is subjected to an RTI in the context of a gamma-ray burst (GRB, Duffell & MacFadyen 2013, 2014). The physical reason for the onset of such an RTI is similar to that of the supernova remnant, except for the velocity of the ejecta shell. This instability may be responsible for amplifying the magnetic field via small-scale turbulent dynamo facilitating the synchrotron emission for the GRB afterglow.

An unstable interface appears in the interaction between stellar and relativistic pulsar winds (Bosch-Ramon et al. 2015; Christie et al. 2016). Since the low-density shocked pulsar wind accelerates the denser shocked stellar wind, RTIs occur at the interface between the shocked winds. The development of such RTIs has a large impact on the evolution of the shocked winds.

Besides the aforementioned topics, the growth of RTIs at the interface between a relativistic jet and its surrounding medium impacts on the stability of the jet structure when the jet either expands radially because of the centrifugal force (Meliani & Keppens 2007, 2009; Millas et al. 2017) or oscillates radially because of a pressure gradient (Matsumoto & Masada 2013; Toma et al. 2017). The stability of relativistic jets is important for the acceleration/deceleration and collimation mechanisms of the GRB, active galactic nucleus (AGN), and microquasar jets.

The stability of the jet interface is also related to the inhomogeneity of the jet and to the evolution of turbulence inside/outside the jet. These processes affect the radiative output from the jet associated with particle and/or photon acceleration. Multiple outflow layers inside a relativistic jet are essential for reproducing the typical observed spectra of GRBs (Ito et al. 2014). The development of turbulence inside the jet is an important issue in any discussion of the mechanism for efficient particle acceleration in the context of GRBs (Asano & Terasawa 2015) and blazars (Asano & Hayashida 2015; Inoue & Tanaka 2016).

Since there is a velocity shear at the interface between the jet and external medium, a promising mechanisms for destabilizing the jet interface are the Kelvin–Helmholtz instability (KHI) and the shear driven instability (e.g., Urpin 2002; Aloy et al. 2002). Many authors have investigated the growth of KHIs at the relativistic flow interface both analytically and numerically (e.g. Turland & Scheuer 1976; Blandford & Pringle 1976; Ferrari et al. 1978; Hardee 1979; Hardee et al. 1998, 2001; Perucho et al. 2004, 2005, 2007; Mizuno et al. 2007; Rossi et al. 2008; Perucho et al. 2010). By comparison, the growth of RTIs at such an interface is not still well understood. Even the general conditions for the onset of the RTI at the jet interface are unclear at present.

The dispersion relation for the relativistic RTI was derived by Allen & Hughes (1984) and Duffell & MacFadyen (2011). However, those studies were limited to the non-relativistic flow of relativistically hot gas. Meliani & Keppens (2009) derived the condition for RTI onset at the interface of the relativistic jet by using an approximate dispersion relation.

Levinson (2010) performed a stability analysis of the two-shock solution (Nakamura & Shigeyama 2006) describing the interaction of relativistic ejecta with an ambient medium and showed that the contact discontinuity between the shocked ejecta and the shocked ambient medium was RT unstable. However, their analysis is not directly applicable to the interface of a relativistic jet. This is because the direction of the normal vector of the contact discontinuity is perpendicular to the relativistic flow in the jet–external-

medium system (considered as a slice transversal to the jet flow, see Fig. 1b) whereas it is parallel to the relativistic flow in the interaction between the relativistic ejecta and the ambient medium.

In this paper, we study the general conditions for the onset and growth of the relativistic RTI at the discontinuous surface of the relativistic flow. For this purpose, we perform a linear analysis and numerical simulations of the RTI in a simple jet–cocoon-medium system, and we compare the analytically derived growth rate to that estimated numerically. Our findings, such as the dispersion relation and the growth rate of the relativistic RTI, are also applicable to analyzing the stability of the interface between stellar and relativistic pulsar winds (Bosch-Ramon et al. 2015; Christie et al. 2016) as well as the stability prospects of the formation of anomalous shear layers in relativistic jets (see, e.g., Aloy & Rezzolla 2006; Aloy & Mimica 2008; Mizuno et al. 2008; Zenitani et al. 2010).

This paper is organized as follows. In Section 2, we present the linear analysis and derive the dispersion relation of the relativistic RTI. In Section 3, we compare RTI growth rates between the analytical model and the numerical simulations. Finally, we summarize and discuss our findings in Section 4.

2 LINEAR ANALYSIS

2.1 Physical assumptions and basic equations

We investigate the stability of the radially oscillating interface between the jet and the cocoon medium. This radial motion of the jet is excited naturally by the pressure mismatch between the jet and its surrounding medium (i.e. the cocoon in typical AGN jets) when the jet propagates through an ambient medium (Sanders 1983; Matsumoto et al. 2012). This oscillatory motion of the jet is the origin of the formation of the reconfinement shocks inside the jet. In the rest frame of the decelerating jet interface that is expanding radially (i.e., in the direction perpendicular to the jet axis), an inertia force acts on the interface and is directed outwards. Therefore, the jet flow is driven against the cocoon in the direction opposite to the inertia force in this frame. We point out that the direction of the jet interface is perpendicular to the relativistic flow of the jet. Figure 1 shows a schematic picture of the jet–cocoon system that we consider in this study. Next, we derive the dispersion relation of the RTI in this system following the standard procedure for the RTI in classical hydrodynamics (Chandrasekhar 1961).

Assuming that magnetic fields are dynamically negligible, the jet–cocoon system can be modeled as an ideal gas subject to the equations of relativistic hydrodynamics, which can be suitably written as

$$\frac{\partial}{\partial t}(\gamma\rho) + \nabla \cdot (\gamma\rho\mathbf{v}) = 0, \quad (1)$$

$$\gamma^2\rho h \left[\frac{\partial \mathbf{v}}{\partial t} + (\mathbf{v} \cdot \nabla)\mathbf{v} \right] = -\nabla P - \frac{\mathbf{v}}{c^2} \frac{\partial P}{\partial t} + \gamma^2\rho h \mathbf{g}, \quad (2)$$

$$\frac{ds}{dt} = 0, \quad (3)$$

where

$$h := 1 + \frac{\Gamma}{\Gamma - 1} \frac{P}{\rho c^2} \quad (4)$$

and

$$s := \log \left(\frac{P^{1/\Gamma-1}}{\rho^{\Gamma/\Gamma-1}} \right) = \frac{1}{\Gamma - 1} \log \frac{P}{\rho^\Gamma}. \quad (5)$$

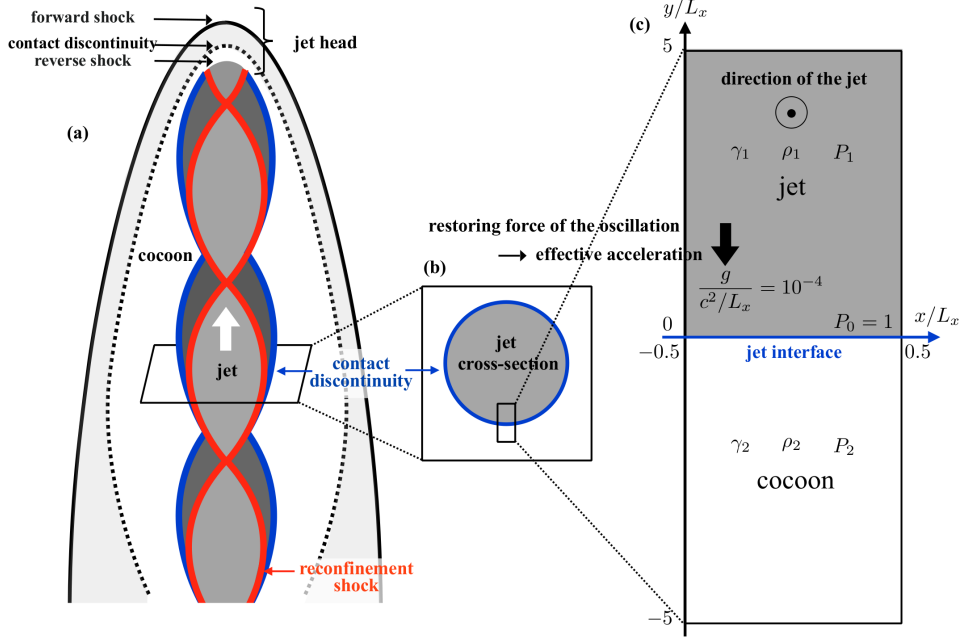


Figure 1. Panel (a): Schematic picture of the jet propagation. Panel (b): Cross-section of the jet. Panel (c): Geometry of the jet–cocoon medium system in the linear stability analysis and numerical simulations. Here, L_x , P_0 and c are the length of the computational domain in the x –direction, P_0 the pressure normalization and c the speed of light in vacuum.

These are the continuity equation (1), the equation of motion (2) and the entropy conservation equation (3). Here, ρ is the rest-mass density, P is the pressure, h is the specific enthalpy, s is the entropy density, Γ is the ratio of specific heats, \mathbf{v} is the velocity vector, $\gamma := (1 - v^2/c^2)^{-1/2}$ is the Lorentz factor, c is the speed of light and \mathbf{g} is the acceleration vector for the inertia force.

In order to simplify the analysis, we assume that the jet radius is large enough that the jet interface can locally be regarded as a planar, rather than a quasi-cylindric surface. With this simplification, we neglect the impact of the curvature of the jet interface on the growth of the RTI. Moreover, this approximation allows us to obtain the sought dispersion relation employing Cartesian coordinates (x, y, z) . The assumed geometry of the jet–cocoon system in the forthcoming linear stability analysis and numerical simulations is sketched in Fig. 1c. The jet beam is shaped by the cocoon when a uniform acceleration is directed in the negative y –direction. The unperturbed jet beam moves in the positive z –axis. The interface between the jet and the cocoon is initially located at $y = 0$. We consider the dynamics only in the x – y plane by assuming that derivatives of the physical variables in the z –direction are zero although the z –component of velocity itself is taken into account. Neglecting the variations in the z –direction means assuming that both, the temporal and the spatial variations of the physical variables along the z –direction are much smaller than in the x – y plane. We will check the validity of this assumption in light of the developments of Sect. 2.4. We anticipate that the KHI can not grow under the previous assumption. In addition, we neglect the temporal variation of the pressure in equation (2) because the pressure gradient force is dominant in the process of the jet oscillation and counterbalances the inertia force in the rest frame of the jet interface. The z –component of velocity, v_z , is not perturbed under these assumptions. This is because there is no external force in the z –direction: $dv_z/dt = 0$. The z –component of velocity contributes only to the Lorentz factor. Since the motion of the fluid in the x – y plane is

much slower than the speed of sound, we assume the fluid is incompressible. Writing the incompressibility condition in component form and added to the governing equations (1)–(3) we obtain:

$$\frac{\partial}{\partial t}(\gamma\rho) + v_x \frac{\partial}{\partial x}(\gamma\rho) + v_y \frac{\partial}{\partial y}(\gamma\rho) = 0, \quad (6)$$

$$\frac{\partial v_x}{\partial x} + \frac{\partial v_y}{\partial y} = 0, \quad (7)$$

$$\gamma^2 \rho h \left(\frac{\partial v_x}{\partial t} + v_x \frac{\partial v_x}{\partial x} + v_y \frac{\partial v_x}{\partial y} \right) = -\frac{\partial P}{\partial x}, \quad (8)$$

$$\gamma^2 \rho h \left(\frac{\partial v_y}{\partial t} + v_x \frac{\partial v_y}{\partial x} + v_y \frac{\partial v_y}{\partial y} \right) = -\frac{\partial P}{\partial y} - \gamma^2 \rho h g, \quad (9)$$

$$\frac{\partial s}{\partial t} + v_x \frac{\partial s}{\partial x} + v_y \frac{\partial s}{\partial y} = 0. \quad (10)$$

Equation (6) is the incompressibility condition for the relativistic gas restricted to motion in the x – y plane.

2.2 Equilibrium state for the linear stability analysis

We assume that the jet–cocoon–medium system is initially in hydrostatic equilibrium in the x – y plane. The pressure gradient counterbalances the inertia force in the y –direction;

$$\frac{\partial P}{\partial y} = -\gamma^2 \rho h g. \quad (11)$$

Assuming that ρ and v_z are uniform and that in the unperturbed estate $v_x = v_y = 0$ in both the jet and in the cocoon regions, the pressure distribution in the initial equilibrium is obtained as fol-

lows:

$$P = P_0 e^{-y/H} + \frac{\Gamma - 1}{\Gamma} \rho c^2 (e^{-y/H} - 1), \quad (12)$$

where P_0 is the pressure at $y = 0$ and

$$H := \frac{\Gamma - 1}{\Gamma} \frac{c^2}{\gamma^2 g} \quad (13)$$

is the pressure scale height determined by the acceleration and the Lorentz factor. Since the inertia force has its origin in the radially oscillating motion of the jet, assuming the amplitude of the jet oscillation is roughly equal to the jet radius, the magnitude of the acceleration g is estimated as follows:

$$g \sim \frac{r_{\text{jet}}}{\tau_{\text{osci}}^2}. \quad (14)$$

Here τ_{osci} is the typical oscillation time of the jet and is given by sound crossing time of the jet radius (Matsumoto et al. 2012):

$$\tau_{\text{osci}} = \gamma_{\text{jet}} r_{\text{jet}} / C_s. \quad (15)$$

Note that γ_{jet} is the typical Lorentz factor of the jet and must be included to compute the sound crossing time in the laboratory frame. The sound speed C_s is maximal and equal to $c/\sqrt{3}$ if the jet is relativistically hot. From equations (13)–(15), we estimate the pressure scale height in the jet region to be larger than the jet radius:

$$H \gtrsim r_{\text{jet}}. \quad (16)$$

Since we neglect the impact of the curvature of the jet radius in this study, everything located at distances $y \gtrsim H$ can be considered as “far” from the jet interface.

2.3 Linearized equations

We investigate the stability of the initial hydrostatic equilibrium between the jet and the cocoon by disturbing the system slightly and following its evolution. We consider the actual density, pressure and velocity components in the perturbed state to be $\rho + \delta\rho$, $P + \delta P$, δv_x and δv_y , respectively. Note that since the perturbed velocity is perpendicular to the unperturbed velocity that has only a z -component, the linearized Lorentz factor in the perturbed state corresponds to that in the unperturbed state. When equations (6)–(10) are linearized, they become

$$\gamma \frac{\partial \delta \rho}{\partial t} + \delta v_y \frac{\partial (\gamma \rho)}{\partial y} = 0, \quad (17)$$

$$\frac{\partial \delta v_x}{\partial x} + \frac{\partial \delta v_y}{\partial y} = 0, \quad (18)$$

$$\gamma^2 \rho h \frac{\partial \delta v_x}{\partial t} = -\frac{\partial \delta P}{\partial x}, \quad (19)$$

$$\gamma^2 \rho h \frac{\partial \delta v_y}{\partial t} = -\frac{\partial \delta P}{\partial y} - \gamma^2 \left(\delta \rho + \frac{\Gamma}{\Gamma - 1} \frac{\delta P}{c^2} \right) g, \quad (20)$$

$$\frac{1}{P} \left(\frac{\partial \delta P}{\partial t} + \delta v_y \frac{\partial P}{\partial y} \right) - \frac{\Gamma}{\rho} \left(\frac{\partial \delta \rho}{\partial t} + \delta v_y \frac{\partial \rho}{\partial y} \right) = 0. \quad (21)$$

As discussed by Allen & Hughes (1984), this set of equations over-constrains the problem in classical cases (Chandrasekhar 1961; Allen & Hughes 1984) because of the additional assumption of fluid incompressibility. Therefore, in those studies, the energy equation was not taken into account because it contains no extra

information. However, the situation here is slightly different from that in previous work. In addition to a density jump, there is a difference in the Lorentz factor across the interface between two fluids. Using equation (17), the linearized equation for the conservation of the entropy (21) is replaced by

$$\frac{\partial \delta P}{\partial t} + \delta v_y \left(\frac{\partial P}{\partial y} + \frac{\Gamma}{\gamma} \frac{\partial \gamma}{\partial y} P \right) = 0. \quad (22)$$

This indicates that in the temporal evolution of the pressure perturbations is triggered by the gradients in the y -direction of both the pressure and also the Lorentz factor. The y -variation of the Lorentz factor is driven by the velocity perturbations δv_y . Since the Lorentz factor is uniform in both the jet and cocoon regions, the gradient of the Lorentz factor in the y -direction should be considered in our model as acting across the jet interface when we derive the dispersion relation for the relativistic RTI.

2.4 Dispersion relation

We assume that the perturbations of physical variables have the Wentzel–Kramers–Brillouin (WKB) spatial and temporal dependence given by $\exp[i(kx - \omega t)]$, where k and ω are the wavenumber in the x -direction and the frequency, respectively. Since we neglect the impact of the curvature of the jet interface, the wavelength of the perturbation in the x -direction is much smaller than the jet radius. Therefore, using equation (16), we obtain

$$\frac{1}{k} \ll H. \quad (23)$$

In addition, the evolution of the perturbed system is faster than the dynamical time of the unperturbed background state,

$$\frac{1}{\omega} \ll \sqrt{\frac{H}{g}}, \quad (24)$$

where $\sqrt{H/g}$ corresponds roughly to the oscillation time scale as can be inferred from equations (14) and (16). The radial oscillations of the jet are advected by the underlying beam in the z -direction, with an advection speed equal to the unperturbed vertical component in the jet velocity, v_z . The temporal and spatial scales in the jet direction are comparable to or larger than those in the radial direction. Therefore, the changes of the background system in the z -direction are also slow and long compared to those of the perturbed system from equations (23) and (24). A posteriori, this justifies neglecting the derivatives of the physical variables with respect to z . Considering the WKB ansatz, equations (17)–(20) and (22) become

$$-i\omega \gamma \delta \rho + \delta v_y D_y (\gamma \rho) = 0, \quad (25)$$

$$ik \delta v_x + D_y \delta v_y = 0, \quad (26)$$

$$-i\omega \gamma^2 \rho h \delta v_x = -ik \delta P, \quad (27)$$

$$-i\omega \gamma^2 \rho h \delta v_y = -D_y \delta P - \gamma^2 \left(\delta \rho + \frac{\Gamma}{\Gamma - 1} \frac{\delta P}{c^2} \right) g, \quad (28)$$

$$-i\omega \delta P + \delta v_y \left(-\frac{\Gamma - 1}{\Gamma} \frac{\rho c^2 h}{H} + \Gamma \frac{D_y \gamma}{\gamma} P \right) = 0, \quad (29)$$

where $D_y := \partial/\partial y$. Note that the second term in equation (29) is given by using equations (11) and (13). Combining equations (28)

and (29) leads to

$$-i\omega\gamma^2\rho h\delta v_y = -D_y\delta P - \gamma^2\delta\rho g + \frac{\gamma^2}{i\omega}\left(\frac{\rho h}{H} - \frac{D_y\gamma}{\gamma}\frac{\Gamma^2}{\Gamma-1}\frac{P}{c^2}\right)g\delta v_y. \quad (30)$$

Eliminating the perturbed density $\delta\rho$, pressure δP and x -component of velocity δv_x in equations (25)–(27) and (30), we obtain the following differential equation for the y -component of velocity in the perturbed state δv_y :

$$\begin{aligned} D_y(\omega^2\gamma^2\rho hD_y\delta v_y) - k^2\omega^2\left(1 - \frac{g}{H\omega^2}\right)\gamma^2\rho h\delta v_y \\ = k^2\gamma\left[D_y(\gamma\rho) + D_y\gamma\frac{\Gamma^2}{\Gamma-1}\frac{P}{c^2}\right]g\delta v_y. \end{aligned} \quad (31)$$

Comparing the typical time scales of the perturbed and unperturbed system, from equation (24), the above differential equation reduces to

$$\begin{aligned} D_y(\omega^2\gamma^2\rho hD_y\delta v_y) - k^2\omega^2\gamma^2\rho h\delta v_y \\ = k^2\gamma\left[D_y(\gamma\rho) + D_y\gamma\frac{\Gamma^2}{\Gamma-1}\frac{P}{c^2}\right]g\delta v_y. \end{aligned} \quad (32)$$

Since the density and Lorentz factor are uniform in the jet and cocoon regions, we may drop the terms $D_y(\gamma\rho)$ and $D_y\gamma$ on the right hand side of equation (32). Using equation (12), we obtain

$$\rho h = \left(\rho + \frac{\Gamma}{\Gamma-1}\frac{P_0}{c^2}\right)e^{-\gamma/H}, \quad (33)$$

relation that can be plugged into equation (32) for both regions of the fluid, leading to

$$D_y^2\delta v_y - \frac{1}{H}D_y\delta v_y - k^2\delta v_y = 0, \quad (34)$$

where we have assumed that ω is constant. The general solution of equation (34) is

$$\delta v_y = Ae^{\alpha_1 y} + Be^{\alpha_2 y}, \quad (35)$$

where

$$\alpha_1 = -k\left(-\frac{1}{2kH} + \sqrt{\frac{1}{4k^2H^2} + 1}\right) \quad (36)$$

and

$$\alpha_2 = k\left(\frac{1}{2kH} + \sqrt{\frac{1}{4k^2H^2} + 1}\right). \quad (37)$$

From equation (23), we drop $1/2kH$ and $1/4k^2H^2$ in equations (36) and (37). Assuming δv_y vanishes when $y \rightarrow \pm\infty$ for the boundaries of δv_y , equation (35) is replaced by

$$\delta v_y = Ae^{-ky} \quad (y > 0) \quad (38)$$

and

$$\delta v_y = Ae^{ky} \quad (y < 0). \quad (39)$$

To ensure the continuity of δv_y across the jet interface ($y = 0$), the same constant A is chosen in the solutions for $y > 0$ and $y < 0$.

The dispersion relation that we require is obtained by plugging equations (38) and (39) into equation (32) and then integrating equation (32) over an infinitesimal element of y across the interface and dropping the integral of the non-divergent term:

$$\omega^2 = -gk\frac{\gamma_1^2\rho_1h_1 - \gamma_2^2\rho_2h_2 + \Gamma(\gamma_1^2 - \gamma_2^2)P_0/c^2}{\gamma_1^2\rho_1h_1 + \gamma_2^2\rho_2h_2} \quad (40)$$

$$= -gk\frac{\gamma_1^2\rho_1h'_1 - \gamma_2^2\rho_2h'_2}{\gamma_1^2\rho_1h_1 + \gamma_2^2\rho_2h_2}. \quad (41)$$

Here, the subscripts 1 and 2 stand for the physical variables in the jet and cocoon region, respectively, and

$$h' := 1 + \frac{\Gamma^2}{\Gamma-1}\frac{P_0}{\rho c^2}. \quad (42)$$

Note that P_0 is the pressure at the jet interface. Its coefficient in the above expression for h' is larger by a factor of Γ than that in the corresponding expression for specific enthalpy h (see equation 4). This is due to considering the difference in the Lorentz factor across the jet interface in equation (22) although there is no difference in pressure.

Instability sets in when $\omega^2 < 0$. Thus, from equation (41), the condition for the onset and growth of the RTI at the relativistic jet interface is given by

$$\gamma_1^2\rho_1h'_1 > \gamma_2^2\rho_2h'_2. \quad (43)$$

The important point for this onset condition is that the difference in effective inertia between two different fluids does not give a criterion for the onset of the RTI. Note that besides the difference in the effective inertia, an additional term $\Gamma(\gamma_1^2 - \gamma_2^2)P_0/c^2$ is necessary for the criterion for the onset of the relativistic RTI.

In the non-relativistic limit ($\gamma \rightarrow 1$, $h \rightarrow 1$ and $h' \rightarrow 1$), the relativistic dispersion relation for the RTI (equation 41) corresponds to the classical one (Chandrasekhar 1961):

$$\omega^2 = -gk\frac{\rho_1 - \rho_2}{\rho_1 + \rho_2}. \quad (44)$$

When we consider the non-relativistic flow of relativistically hot gas ($h > 1$ and $\gamma = 1$, Allen & Hughes 1984), this reduces to

$$\omega^2 = -gk\frac{\rho_1 - \rho_2}{\rho_1 + \rho_2 + 2\Gamma/(\Gamma-1)P_0/c^2}. \quad (45)$$

In both classical cases, the difference in rest-mass density between the two fluids drives the RTI.

The temporal growth rate σ is defined as the imaginary part of the frequency:

$$\sigma := \text{Im } \omega. \quad (46)$$

The dimensionless growth rate is given by

$$\frac{\sigma}{\sqrt{gk}} = \sqrt{\mathcal{A}}, \quad (47)$$

where \mathcal{A} is the Atwood number, which is a non-dimensional parameter that characterizes the linear growth of the RTI. In the relativistic case, from equation (40), one can find

$$\mathcal{A} = \frac{\gamma_1^2\rho_1h_1 - \gamma_2^2\rho_2h_2 + \Gamma(\gamma_1^2 - \gamma_2^2)P_0/c^2}{\gamma_1^2\rho_1h_1 + \gamma_2^2\rho_2h_2}. \quad (48)$$

When the Lorentz factor of the jet is much larger than that of the cocoon ($\gamma_1 \gg \gamma_2$) and the pressure at the jet interface is relativistic ($P_0 \gg \rho_1c^2, \rho_2c^2$), the Atwood number is almost equal to the ratio of specific heats:

$$\mathcal{A} \sim \Gamma. \quad (49)$$

This is greater than unity when we consider $\Gamma > 1$, for example, the ideal-gas case ($\Gamma = 4/3$). In contrast, the classical Atwood number is always less than unity, because its denominator is greater than its numerator (see equations 44 and 45).

3 NUMERICAL STUDY OF STABILITY OF INTERFACE BETWEEN JET AND COCOON

We perform numerical simulations to investigate the stability of the interface separating the jet from the cocoon and the growth of the RTI at the jet interface. In particular, we verify the dispersion relation of the RTI derived analytically in the previous section by comparing the linear growth rates in the analytic model and the numerical simulations.

3.1 Governing equations

The set up we consider in this section is almost the same as that in Section 2.1. Figure 1c shows the initial geometry of the jet–cocoon–medium system schematically. The jet beam is on top of the cocoon and it is subject to a uniform acceleration driven by the restoring force sketched with a thick black arrow in Fig. 1c. We solve the evolution of this system numerically by assuming a small amplitude for the corrugated jet interface.

Assuming an ideal gas equation of state with a constant ratio of specific heats $\Gamma = 4/3$, the governing equations to be solved are

$$\frac{\partial}{\partial t}(\gamma\rho) + \frac{\partial}{\partial x}(\gamma\rho v_x) + \frac{\partial}{\partial y}(\gamma\rho v_y) = 0, \quad (50)$$

$$\frac{\partial}{\partial t}(\gamma^2\rho h v_x) + \frac{\partial}{\partial x}(\gamma^2\rho h v_x v_x + P) + \frac{\partial}{\partial y}(\gamma^2\rho h v_x v_y) = 0, \quad (51)$$

$$\frac{\partial}{\partial t}(\gamma^2\rho h v_y) + \frac{\partial}{\partial x}(\gamma^2\rho h v_y v_x) + \frac{\partial}{\partial y}(\gamma^2\rho h v_y v_y + P) = -\gamma^2\rho h g, \quad (52)$$

$$\frac{\partial}{\partial t}(\gamma^2\rho h v_z) + \frac{\partial}{\partial x}(\gamma^2\rho h v_z v_x) + \frac{\partial}{\partial y}(\gamma^2\rho h v_z v_y) = 0, \quad (53)$$

$$\frac{\partial}{\partial t}(\gamma^2\rho h c^2 - P) + \frac{\partial}{\partial x}(\gamma^2\rho h c^2 v_x) + \frac{\partial}{\partial y}(\gamma^2\rho h c^2 v_y) = -\gamma^2\rho h g v_y, \quad (54)$$

where the symbols are defined as in Section 2. Any derivatives of a physical variable in the z -direction are assumed to be zero. The impact on the system of the inertia force in the y -direction is included in the source terms in both the momentum and energy conservation equations. The time evolution of v_z and the temporal variation of the pressure are considered in equations (53) and (54), respectively, although we did not take them into account in the previous section.

A relativistic HLLC scheme (Mignone & Bodo 2005) is used to solve equations (50)–(54) in conserved form. The primitive variables are calculated from the conservative variables following the method of Mignone & McKinney (2007). Second order accuracy is obtained in our code by employing an spatial MUSCL-type intercell reconstruction and a second-order Runge–Kutta time integration. See Matsumoto et al. (2012) and Matsumoto & Masada (2013) for the details of our special relativistic hydrodynamic (SRHD) code.

3.2 Initial setting of jet–cocoon–medium system

The jet–cocoon system is initially in hydrostatic equilibrium in the x – y plane (see Section 2.2 and Fig. 1c for details). The computational domain consists of a rectangle with x – and y –dimensions L_x and $L_y = 10L_x$, respectively, covered with a uniform grid with the same mesh spacing in both directions ($\Delta x = \Delta y$). Three different resolutions ($\Delta x/L_x = 0.0025, 0.005$ and 0.01) are used to

Table 1. Rest-mass density of the cocoon in hydrostatic equilibrium, ρ_2 , for all models is listed. The rest-mass density of the jet and the Lorentz factor of the jet and the cocoon are fixed in all models. We set $\rho_1 = 0.1$, $\gamma_1 = 5$, and $\gamma_2 = 1$. The corresponding relativistic Atwood number \mathcal{A} for each model is also listed. In addition, the dimensionless growth rate σ/\sqrt{gk} evaluated from numerical results are shown in this table. Here, $gk = 2\pi \times 10^{-4}$.

	ρ_2	\mathcal{A}	σ/\sqrt{gk}
Model A (fiducial)	1	1.2	1.081
Model B	12	1.0	0.969
Model C	25.2	0.8	0.892
Model D	41.6	0.6	0.753
Model E	62.8	0.4	0.625
Model F	91.0	0.2	0.422

test the convergence of the growth rate of the RTI for the fiducial model. For other models, we use $\Delta x/L_x = 0.01$. Periodic boundary and outflow (zero gradient) conditions are set in the x – and y –directions, respectively.

The normalization units for length, velocity, time and energy density are chosen as L_x , the speed of light c , the light-crossing time over the length of the calculation domain in the x –direction, L_x/c , and the pressure at the jet interface, P_0 , respectively. In the following, we set $c = 1$. The upper ($0 < y < 5L_x$) and lower ($-5L_x < y < 0$) regions are filled with the jet and cocoon media, respectively. We set $P_0 = 1$ at the jet interface located at $y = 0$, and at every other point in the domain, we employ equation (12). The jet propagation direction is taken to be the z –direction. Following the convention stated in the previous section, subscripts 1 and 2 stand for the physical variables in the jet and cocoon regions, respectively. In the following, we fix the pressure at the jet interface, P_0 , the physical variables of the jet (γ_1 and ρ_1) and the Lorentz factor of the cocoon, γ_2 . The Lorentz factor and rest-mass density of the jet are $\gamma_1 = 5$ and $\rho_1 = 0.1$, respectively. This sets the jet as mildly relativistic in terms of internal energy. This initialization has been set up for numerical convenience, but our stability analysis does not critically depend on the exact ratio of kinetic to thermal energy in the jet or in the cocoon, as we shall see. The Lorentz factor of the cocoon is $\gamma_2 = 1$. This means that the velocity of the cocoon is zero, consistent with the fact that the cocoon is in hydrostatic equilibrium. The rest-mass density of the cocoon, ρ_2 , depends on the model. In the fiducial model, we set $\rho_2 = 1$, which makes this model mildly relativistic from the thermodynamics viewpoint. In the growth of the RTI, the Atwood number \mathcal{A} is an important parameter with which to investigate the evolution of the system. We set $\mathcal{A} = 1.2$ in the fiducial model (equation 48). In order to compare the dimensionless growth rates of the analytic model and the numerical simulations, we consider six cases: $\mathcal{A} = 0.2, 0.4, 0.6, 0.8, 1.0$ and 1.2 . The Atwood number and the corresponding density of the cocoon in hydrostatic equilibrium for all models are listed in Table 1. The set of models we consider span a useful range of Atwood numbers by changing the value of the density of the cocoon (ρ_2). For this range of Atwood numbers, it turns out that the cocoons of our relativistic jets are only mildly relativistic or subrelativistic, since $P_0/\rho_2 \lesssim 1$.

As described in Section 2.2, the inertia force originates from the radial oscillations of the jet. From equations (13) and (16), we

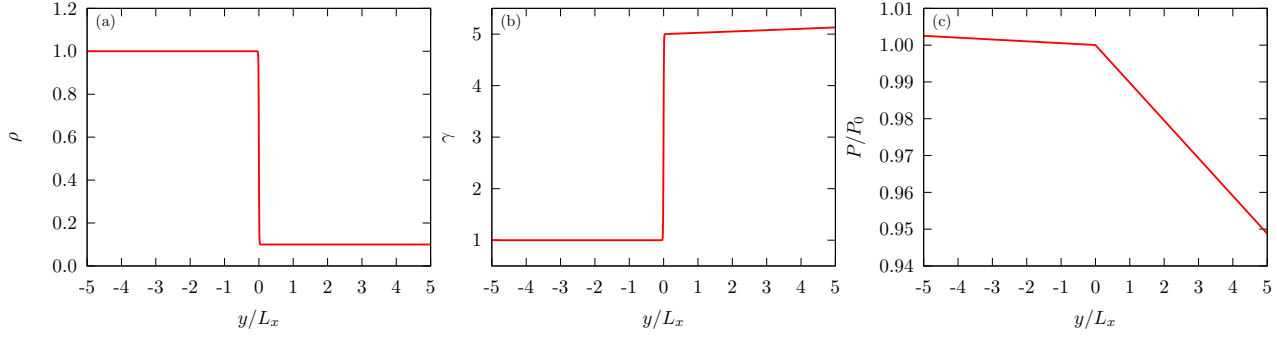


Figure 2. Initial spatial distributions of (a) rest-mass density, (b) Lorentz factor and (c) pressure in the y -direction for the fiducial model when $\Delta x/L_x = w/L_x = 0.01$.

can obtain the following relationship:

$$gL_x \sim \frac{\Gamma}{\Gamma - 1} \frac{1}{\gamma_{\text{jet}}^2} \frac{L_x}{r_{\text{jet}}} = 10^{-4} \left(\frac{5}{\gamma_1} \right)^2 \left(\frac{100}{r_{\text{jet}}/L_x} \right). \quad (55)$$

Since the impact of the curvature of the jet interface is neglected in this study, assuming $r_{\text{jet}} = 100L_x$, we set the normalized acceleration gL_x to 10^{-4} .

The jet-cocoon system is disturbed by a small amplitude perturbations of the y -component of velocity in the form of

$$v_y(x, y) = \frac{\delta v}{4} \left[1 - \cos\left(\frac{2\pi x}{L_x}\right) \right] \left[1 + \cos\left(\frac{2\pi y}{10L_x}\right) \right], \quad (56)$$

corresponding to $k = 2\pi/L_x$. Indeed, the horizontal domain length, L_x , is set to coincide with a full wavelength of the perturbation introduced. We take $\delta v = 10^{-4}$ in all our models. To exclude the growth of random perturbations with wavelengths of the order of the grid size, we set smooth transition profiles for the density and effective inertia in the y -direction at the jet interface as follows:

$$\rho(y) = \frac{1}{2} \left[\rho_1 + \rho_2 + (\rho_1 - \rho_2) \tanh\left(\frac{y}{w}\right) \right], \quad (57)$$

$$I(y) = \frac{1}{2} \left[\gamma_1^2 \rho_1 h_1 + \gamma_2^2 \rho_2 h_2 + (\gamma_1^2 \rho_1 h_1 - \gamma_2^2 \rho_2 h_2) \tanh\left(\frac{y}{w}\right) \right]. \quad (58)$$

Here, $I(y)$ is the spatial distribution of the effective inertia in the y -direction. w is a parameter that controls the width of the jet interface, which should be much smaller than the wavelength of the perturbation: we set $w/L_x = 0.01$. The effective width of the interface is roughly $4w$ considering the functional dependence of the transition layer from equation (57). Since the spatial distribution of the effective inertia in the y -direction is given by equation (58), the pressure distribution in hydrostatic equilibrium in the calculation domain is obtained by integrating the balancing equation (11):

$$P(y) = \int -I(y)g dy. \quad (59)$$

Using the spatial distributions of the rest-mass density, effective inertia and pressure, the Lorentz factor also has a smooth transition profile as follows:

$$\gamma(y) = \sqrt{\frac{I(y)}{\rho(y) + 4P(y)/c^2}}. \quad (60)$$

For the fiducial model, the initial spatial distributions of the density, the Lorentz factor and the pressure in the whole calculation domain are shown in Figs. 2a, 2b and 2c, respectively.

3.3 Results

The growth of the single RT-mode at the interface of the relativistic jet is investigated by two-and-a-half dimensional SRHD simulations. In order to verify the dispersion relation (41) derived in the previous section, we focus mainly on the linear growth phase of the RTI in the numerical simulations, comparing the temporal growth rates in the analytical model and in the simulations.

The initial spatial distributions of the rest-mass density and effective inertia around the jet interface in the x - y plane for the fiducial model with the resolution $\Delta x/L_x = 0.01$ are shown in panels (a) and (b) of Fig. 3, respectively. The inertia force and the relativistic jet are directed in the negative y -direction and the z -direction, respectively. The lower-density medium of the jet is located above the higher-density medium of the cocoon. In the non-relativistic regime, the RTI is not expected to grow in such a case. However, the effective inertia of the jet is larger than that of the cocoon, even though the jet-to-cocoon density ratio $\rho_1/\rho_2 < 1$. Since the jet has a relativistic velocity and is relativistically hot whereas the cocoon has a non-relativistic velocity and is mildly hot in this model, the Lorentz factor and the relativistic thermal energy help to enhance the inertia of the jet. Therefore, the effectively heavy medium of the jet is on top of the cocoon medium against which the inertia force is pointing. In such a relativistic situation, the RTI can grow at the jet interface. Figure 3c shows the temporal evolution of the spatial distribution of the Lorentz factor. The amplitude of the corrugated interface grows with time because of the growth of the RTI during the linear phase ($t \lesssim 150$). We find a mushroom-like structure in the nonlinear regime ($t = 350$) of the RTI.

The linear growth rates of the relativistic RTI in the analytical model and the numerical simulation of the fiducial model are compared in Fig. 4. The vertical and horizontal axes represent the maximum x -component of velocity in the jet region $v_{x,\text{max}}$ and the time t , respectively. To exclude the impact of the smooth transition region between the jet and cocoon on the linear growth rate of the RTI, we operatively define the jet beam as the region in which the Lorentz factor is greater than 90% of the Lorentz factor of the jet, that is, $\gamma \geq 4.5$. The temporal evolution of $v_{x,\text{max}}$ in the relativistic jet beam is a good indicator for evaluating the linear growth rate of the RTI from the results of the numerical simulations. The value of $v_{x,\text{max}}$ in the relativistic jet beam saturates at the nonlinear stage, whereas the RT bubble and finger are accelerated in the y -direction by the inertia force even in the nonlinear phase, and the amplitude of the y -component of the perturbed velocity continues to grow. The maximum x -component of velocity is plotted every 10 time units (crosses in Fig. 4). The dispersion relation of the relativistic

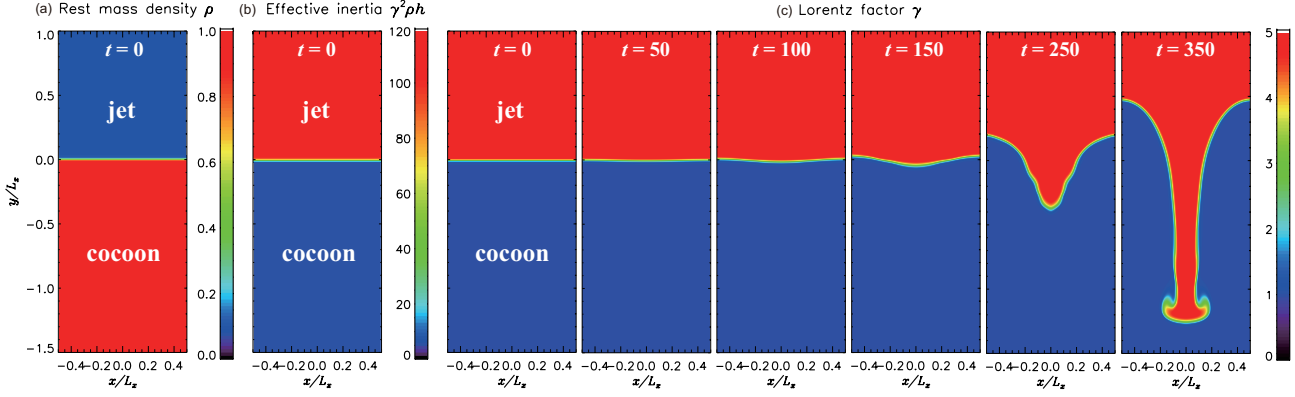


Figure 3. Panel (a): Initial spatial distribution of the rest-mass density. Panel (b): Initial spatial distribution of effective inertia. Panel (C): Temporal evolution of the spatial distribution of Lorentz factor around the jet interface in the x - y plane for the fiducial model. The relativistic jet is directed in z -direction (pointing towards the reader from the plane of the page). The jet beam and the cocoon are represented in the upper and lower parts of the represented panels.

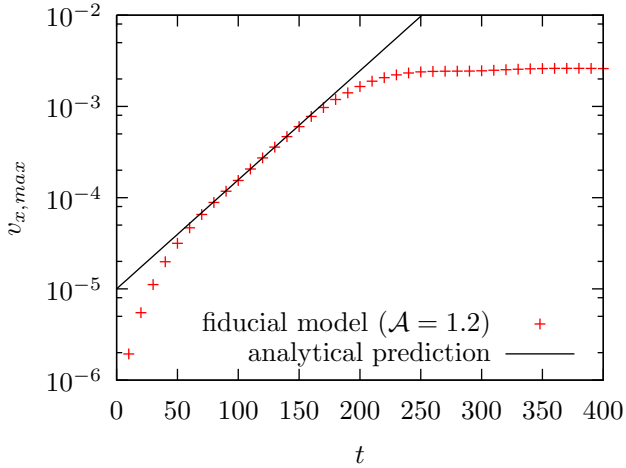


Figure 4. Temporal evolution of the maximum x -component of velocity in the jet region for the fiducial model ($\mathcal{A} = 1.2$). The solid line shows the analytical prediction of $v_{x,max} \propto \exp(\sigma t)$.

RTI (41) predicts $v_{x,max} \propto \exp(\sigma t)$, where σ is the temporal growth rate given by equation (46). This analytical prediction is also shown as the solid line in Fig. 4.

In the early phase of the evolution of the disturbed jet interface, the vertical deformation of the interface occurs between the smooth transition profiles in the y -direction of the density, effective inertia and Lorentz factor because of the inertia force. This results in the deceleration of the y -component of the perturbed velocity, contrary to the expectation. The y -component of velocity begins to accelerate after $t \sim 30$. The x -component of velocity is accelerated from the beginning in contrast to the y -component of velocity. However, the eigenstate of the RTI for the single-wavelength mode we set ($k = 2\pi/L_x$) is not formed in the deceleration phase of the y -component of velocity. Therefore, the growth rate of $v_{x,max}$ is different from the analytical prediction in the early phase of the evolution, which is a kind of relaxation phase of the initial conditions of the numerical simulation. After the eigenstate of the single-mode RTI is fully achieved ($t \geq 50$), we find in Fig. 4 that the growth rates in the analytical prediction from the dispersion relation and in the numerical simulation are almost the same.

The temporal evolution of $v_{x,max}$ in the relativistic jet beam

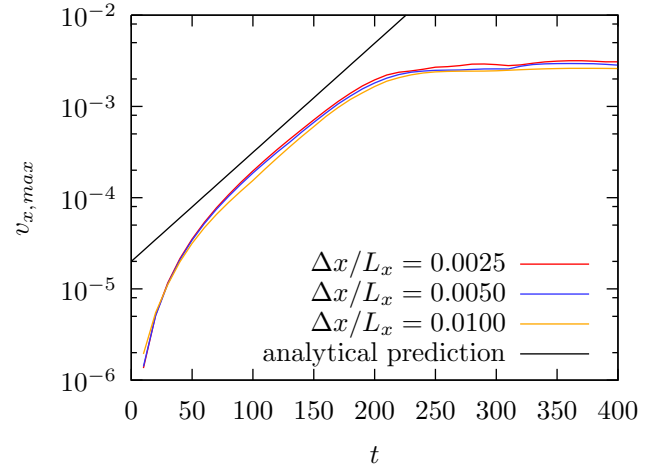


Figure 5. Grid-resolution dependence on the linear growth rate of the RTI for the fiducial model. The initial value of the analytical prediction is twice as large as that shown in Fig. 4.

for the fiducial model with three different resolutions are shown in Fig. 5. The red, blue and orange solid lines represent the cases $\Delta x/L_x = 0.0025, 0.005$ and 0.01 , respectively. The analytically predicted temporal evolution of $v_{x,max}$ is also shown by a black solid line, for reference. Note that since we have freedom to set the normalization of the relation $v_{x,max} \propto \exp(\sigma t)$, the initial value of $v_{x,max}$ in the analytical prediction is taken to be twice as large as that shown in Fig. 4. The growth rate (i.e. the slope of the line during the linear regime) converges for the three different resolutions. Therefore, the coarsest resolution $\Delta x/L_x = 0.01$ is sufficient for calculating the linear growth rate of the relativistic RTI for the fiducial model although the numerical run with the lower resolution takes slightly longer to achieve saturation of the maximum x -component of velocity.

Figure 6 shows the linear growth rates of the relativistic RTI in the analytical model and the numerical runs for all models when $\Delta x/L_x = 0.01$. The vertical and horizontal axes represent the dimensionless growth rate and the Atwood number, respectively. The Atwood number characterizes the linear growth of the RTI and is defined by equation (48) in the relativistic jet-cocoon system. The theoretical relationship between the dimensionless growth rate and

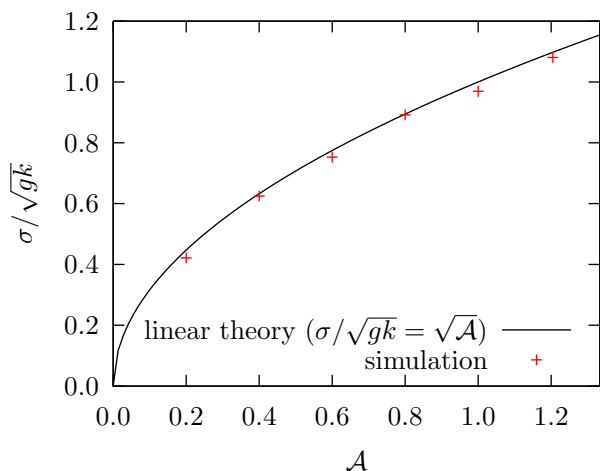


Figure 6. Comparison of the dimensionless growth rates of the relativistic RTI in the linear theory and numerical simulations. The solid line shows the theoretical relation between the relativistic Atwood number and the dimensionless growth rate given by equation (47): $\sigma/\sqrt{gk} = \sqrt{A}$. Red crosses are results of numerical runs and their values are listed in Table 1.

the Atwood number is given by equation (47) and is shown by the solid line in Fig. 6. The crosses represent the dimensionless growth rate of the maximum x -component of velocity between the numerical runs; this is evaluated by fitting the data to an exponential function. In order to prevent the fits to be affected by the initial numerical transient, they are made from a time after which the eigenstate of the single-mode RTI is fully achieved, as listed in Table 1. Note that the Atwood number of the fiducial model, $A = 1.2$, is larger than the maximum one in the classical limit (namely, $A = 1$; Section 2.4). We find from Fig. 6 that our derived dispersion relation predicts the linear growth rate of the relativistic RTI correctly, not only for the fiducial model but also for the rest models.

4 SUMMARY AND DISCUSSION

We have studied the linear stability of an interface between the jet and the cocoon when the jet is forced to oscillate radially. This radial oscillatory motion of the jet is excited naturally by the pressure mismatch between the jet and cocoon media as the jet propagates through the ambient medium. In the rest frame of the decelerating jet interface that is expanding radially, an outward inertia force acts on the interface. This situation is physically equivalent to one in which the jet beam is supported above the cocoon and the former is subject to an effective acceleration. We have performed a linear stability analysis of this system in the absence of viscous effects and derived the dispersion relation.

As in the classical case (Chandrasekhar 1961; Allen & Hughes 1984), the jet interface becomes RT unstable when the jet medium is effectively heavier than the cocoon medium. However, unlike in classical cases, not only the difference in the rest-mass density between the jet and the cocoon, but also the difference in the effective inertia is the relevant quantity to drive an RTI in the relativistic regime. Thus, even if the jet is lighter than the surrounding medium and pressured matched, a sufficiently fast beam becomes effectively heavier than the cocoon and, thus, it is prone to the RTI.

By using an approximate dispersion relation, Meliani & Keppens (2009) showed that a difference in the

effective inertia between two fluids separated by an interface was a criterion for the onset and growth of the relativistic RTI. This is correct when both of fluids are cold, that is, the rest-mass energy is much larger than the thermal energy and the pressure does not contribute to the fluid inertia. Our derived dispersion relation indicated that besides the difference in the effective inertia, an additional pressure term was necessary for the general onset condition of the relativistic RTI. This additional term originated from the advection of the pressure by the gradient of the Lorentz factor across the interface.

The temporal growth rate of the relativistic RTI in the inviscid case is also proportional to the square root of the product of the wavenumber and effective acceleration as it is in the classical case. Therefore, the temporal growth of the shorter-wavelength modes is faster. On the other hand, the dimensionless growth rate normalized by \sqrt{gk} is given by the square root of the relativistic Atwood number, which is determined by only physical variables of the jet and cocoon. The relativistic Atwood number is the most important parameter, characterizing the linear growth of the relativistic RTI. Its maximum value is the ratio of specific heats when the Lorentz factor of the jet is much larger than that of the cocoon and the pressure at the jet interface is relativistic. The Atwood number is greater than unity in this case, as opposed to the classical case, for which it is always smaller than one. This physical condition is expected to be satisfied when the effective inertia of the jet is much smaller than that of the ambient medium in which the jet propagates through. This is because in such a case, the jet is surrounded by a thick and relativistically hot cocoon heated at the strong reverse shock of the jet head (see Fig. 1a).

The relativistic RTI does not grow only at the interface between the jet and its cocoon. Once the jet oscillates radially because of the pressure mismatch between the jet and a surrounding medium, any jet interface except the contact discontinuity at the jet head becomes RT unstable (e.g., “naked jet”, Toma et al. 2017). A remarkable result of our study is that the interface between different components of the jet is generically unstable regardless of the inertia force that drives the RTI. This is due to the fact that the instability condition (43) is expected to hold in relativistic astrophysical jets. Such inertia force can be originated by the pressure gradient considered in this paper or by a centrifugal force if the beam flow is rotating (e.g., Meliani & Keppens 2007, 2009; Martí 2015; Millas et al. 2017). The dispersion relation and growth rate of the relativistic RTI derived in this work are also applicable to the stability analysis of the surfaces limiting the beam of relativistic flows in other astrophysical scenarios (e.g., Bosch-Ramon et al. 2015).

In addition to the linear analysis, the linear growth of the single-mode RTI at the interface of the relativistic jet has been investigated by two-and-a-half dimensional SRHD simulations within a periodic computational box in the direction tangential to the jet interface. The numerical set up that we study by means of numerical simulations was almost the same as that employed in the linear stability analysis of the jet–cocoon system. In our fiducial model, the pressure at the jet interface is mildly relativistic; the Lorentz factors of the jet and cocoon are 5 and 1, respectively. The corresponding relativistic Atwood number is 1.2. The RTI has grown at the jet interface, even though the beam of the jet has lower rest-mass density than the cocoon in the fiducial model. This is because the jet beam is effectively heavier than the cocoon because of the enhanced inertia of the former due to its larger Lorentz factor and specific enthalpy. The validity of our derived dispersion relation is confirmed by a parametric study of different cocoons with

distinct relativistic Atwood numbers, comparing the linear growth rates in the analytical model and numerical simulations.

In this work, we have focused on the linear stability of the jet interface restricted to motions perpendicular to the jet flow and excluding the destabilizing effect of the KHI that grows along the jet direction. Further study of the nonlinear regime of the RTI is necessary to quantify the stability of the oscillating jet interface. In addition, since there shall be a velocity shear at the jet interface in realistic jets, the growth of the KHI plays an important role in their stability (see, e.g., Hardee & Hughes 2003). The nonlinear evolution of the relativistic RTI at the jet interface and the relationship between the KHI and RTI are without the scope of our work and will be reported in our subsequent paper. However, here we may anticipate an interesting result. We note that the instability condition (43) can be rewritten as

$$\eta_{\text{Rc}}^* := \frac{\rho_1 h_1' \gamma_1^2}{\rho_2 h_2' \gamma_2^2} > 1 \quad (61)$$

A parameter formally similar to η_{Rc}^* was defined in Martí et al. (1997) as the key to differentiate morpho-dynamical properties of relativistic jets, namely

$$\eta_{\text{R}}^* := \frac{\rho_1 h_1' \gamma_1^2}{\rho_a h_a' \gamma_a^2}, \quad (62)$$

where the subscript “a” refers to quantities of the ambient medium. Large values of η_{R}^* yield relatively smooth and featureless jets, while relativistic jets inflate large cocoons and develop beams with numerous recollimation shocks in the regime $\eta_{\text{R}}^* \ll 1$, according to Martí et al. (1997). Indeed, Hardee & Hughes (2003), find that $\eta_{\text{R}}^* \gg 1$ is essential to prevent the development of the KHI. We note that our parameter η_{Rc}^* is linked to η_{R}^* through

$$\eta_{\text{Rc}}^* = \eta_{\text{R}}^* \frac{h_1'}{h_1} \frac{\rho_a h_a' \gamma_a^2}{\rho_2 h_2' \gamma_2^2}. \quad (63)$$

Here, $h_1'/h_1 \approx 1$. Since typically the ambient medium is at rest ($\gamma_a = 1$), is cold ($h_a \approx 1$) and (much) denser than the cocoon ($\rho_a/\rho_2 \gg 1$), the fraction $\rho_a h_a' \gamma_a^2/(\rho_2 h_2' \gamma_2^2) \approx \rho_a/(\rho_2 h_2' \gamma_2^2)$ in equation (63) is typically of the order of or larger than unity. This means that the regime in which $\eta_{\text{R}}^* \gg 1$, we also expect $\eta_{\text{Rc}}^* \gg 1$. Hence, the regime in which the KHI is absent, because the effective inertia of the jet beam is much larger than that of the external medium, is optimal for the development of the RTI at the jet/cocoon interface although a driving force for a radial motion of the jet is necessary.

Another interesting consequence of our analysis comes from the fact that the parameter $\eta_{\text{R}}^* = 1$ sets the boundary between non-relativistic and relativistic jet propagation regimes (e.g., Matzner 2003; Bromberg et al. 2011). Even more, $\eta_{\text{R}}^* > \theta_j^{-4/3} \gg 1$ (where θ_j is the jet opening angle), defines the border between uncollimated and collimated jets (e.g., Bromberg et al. 2011). With the same reasoning than in the previous paragraph, in the relativistic jet propagation regime as well as in the uncollimated jet regime, the jet/cocoon interface is expected to be RTI.

Finally, we point out that the development of the RTI can be affected by the existence of gradients in the properties of jets in the across the jet section. The interaction of extragalactic jets with their environment leads to the stratification of the beam of the jet in the direction normal to its velocity (e.g., Perucho & Lobanov 2007; Aloy & Mimica 2008; Hervet et al. 2017) In such cases, we do not have a single Atwood number characterizing the jet’s beam. Instead, a spectrum of Atwood numbers may exist, depending on the exact stratification of the hydrodynamic properties in the boundary

layer between the jet and the external medium. We will address the development of the RTI in these cases in a future work.

ACKNOWLEDGMENTS

We thank Y. Masada, H. R. Takahashi, A. Hillier, A. Mizuta, S. Nagataki, S. S. Komissarov, A. MacFadyen and J. M. Martí for useful discussions. The numerical computations were carried out on a Cray XC30 at the Center for Computational Astrophysics at the National Astronomical Observatory of Japan and on a Cray XC40 at YITP at Kyoto University. This work was supported by JSPS KAKENHI Grant Number JP 17K14308 and in part by the Center for the Promotion of Integrated Sciences (CPIS) of Sokendai. MP acknowledges support by the Spanish “Ministerio de Economía y Competitividad” grant AYA2013-48226-C3-2-P. MAA acknowledges support from the European Research Council (grant CAMAP-259276) and the grants AYA2015-66899-C2-1-P and PROMETEOII/2014-069.

REFERENCES

- Allen, A. J., & Hughes, P. A. 1984, MNRAS, 208, 609
- Aloy, M.-A., Ibáñez, J.-M., Miralles, J.-A., & Urpin, V. 2002, A&A, 396, 693
- Aloy, M. A., Rezzolla, L. 2006, ApJL, L119
- Aloy, M. A., Mimica, P. 2008, ApJ, 681, 84
- Asano, K., & Hayashida, M. 2015, ApJL, 808, L18
- Asano, K., & Terasawa, T. 2015, MNRAS, 454, 2242
- Blandford, R. D., & Pringle, J. E. 1976, MNRAS, 176, 443
- Bosch-Ramon, V., Barkov, M. V., & Perucho, M. 2015, A&A, 577, A89
- Bromberg O., Nakar E., Piran T., Sari R. 2011, ApJ, 740, 100
- Chandrasekhar, S. 1961, International Series of Monographs on Physics, Oxford: Clarendon, 1961,
- Chevalier, R. A. 1976, ApJ, 207, 872
- Christie, I. M., Petropoulou, M., Mimica, P., Giannios, D. 2016, MNRAS, 459, 2420
- Duffell, P. C., & MacFadyen, A. I. 2011, ApJS, 197, 15
- Duffell, P. C., & MacFadyen, A. I. 2013, ApJ, 775, 87
- Duffell, P. C., & MacFadyen, A. I. 2014, ApJL, 791, L1
- Ebisuzaki, T., Shigeyama, T., & Nomoto, K. 1989, ApJL, 344, L65
- Ferrand, G., Decourchelle, A., & Safi-Harb, S. 2012, ApJ, 760, 34
- Ferrari, A., Trussoni, E., & Zaninetti, L. 1978, A&A, 64, 43
- Guo, F., Li, S., Li, H., et al. 2012, ApJ, 747, 98
- Hachisu, I., Matsuda, T., Nomoto, K., & Shigeyama, T. 1992, ApJ, 390, 230
- Hardee, P. E. 1979, ApJ, 234, 47
- Hardee, P. E., & Norman, M. L. 1988, ApJ, 334, 70
- Hardee, P. E., Rosen, A., Hughes, P. A., & Duncan, G. C. 1998, ApJ, 500, 599
- Hardee, P. E., & Hughes, P. A. 2003, ApJ, 583, 116
- Hardee, P. E., Hughes, P. A., Rosen, A., & Gomez, E. A. 2001, ApJ, 555, 744
- Hervet, O., Meliani, Z., Zech, A., et al. 2017, arXiv:1705.10556
- Hillier, A., Isobe, H., Shibata, K., & Berger, T. 2011, ApJL, 736, L1
- Hillier, A., Berger, T., Isobe, H., & Shibata, K. 2012, ApJ, 746, 120
- Hillier, A. S. 2016, MNRAS, 462, 2256

- Inoue, Y., & Tanaka, Y. T. 2016, *ApJ*, 828, 13
- Isobe, H., Miyagoshi, T., Shibata, K., & Yokoyama, T. 2005, *Nature*, 434, 478
- Isobe, H., Miyagoshi, T., Shibata, K., & Yokoyama, T. 2006, *PASJ*, 58, 423
- Ito, H., Nagataki, S., Matsumoto, J., et al. 2014, *ApJ*, 789, 159
- Jun, B.-I., Norman, M. L., & Stone, J. M. 1995, *ApJ*, 453, 332
- Jun, B.-I., & Norman, M. L. 1996, *ApJ*, 465, 800
- Kifonidis, K., Plewa, T., Janka, H.-Th., Müller, E. 2003, *A&A*, 408, 621
- Levinson, A. 2010, *Geophysical and Astrophysical Fluid Dynamics*, 104, 85
- Mao, J., Ono, M., Nagataki, S., et al. 2015, *ApJ*, 808, 164
- Martí, J. M., Müller, E., Font, J. A., Ibáñez, J. M.; Marquina, A. 1997, *ApJ*, 479, 151
- Martí, J. M. 2015, *MNRAS*, 452, 3105
- Matsumoto, J., Masada, Y., & Shibata, K. 2012, *ApJ*, 751, 140
- Matsumoto, J., & Masada, Y. 2013, *ApJL*, 772, L1
- Matzner, C. D. 2003, *MNRAS*, 345, 574
- Meliani, Z., & Keppens, R. 2007, *A&A*, 475, 785
- Meliani, Z., & Keppens, R. 2009, *ApJ*, 705, 1594
- Mignone, A., & Bodo, G. 2005, *MNRAS*, 364, 126
- Mignone, A., & McKinney, J. C. 2007, *MNRAS*, 378, 1118
- Millas, D., Keppens, R., & Meliani, Z. 2017, *MNRAS*, 470, 592
- Mizuno, Y., Hardee, P., & Nishikawa, K.-I. 2007, *ApJ*, 662, 835
- Mizuno, Y., Hardee, P., Hartmann, D. H., Nishikawa, K.-I., & Zhang, B. 2008, *ApJ*, 672, 72-82
- Nakamura, K., & Shigeyama, T. 2006, *ApJ*, 645, 431
- Obergaulinger, M., Iyudin, A. F., Müller, E., & Smoot, G. F. 2014, *MNRAS*, 437, 976
- Obergaulinger, M., Chimento, J. M., Mimica, P., Aloy, M. A., & Iyudin, A. 2014, *HEDP*, 17, 92
- Ono, M., Nagataki, S., Ito, H., et al. 2013, *ApJ*, 773, 161
- Perucho, M., Hanasz, M., Martí, J. M., & Sol, H. 2004, *A&A*, 427, 415
- Perucho, M., Martí, J. M., & Hanasz, M. 2005, *A&A*, 443, 863
- Perucho, M., Hanasz, M., Martí, J.-M., & Miralles, J.-A. 2007, *Phys. Rev. E*, 75, 056312
- Perucho, M., & Lobanov, A. P. 2007, *A&A*, 469, L23
- Perucho, M., Martí, J. M., Cela, J. M., et al. 2010, *A&A*, 519, A41
- Rayleigh, L. 1900, *Scientific Papers*, Vol. II (Cambridge: Cambridge Univ. Press), 200
- Rossi, P., Mignone, A., Bodo, G., Massaglia, S., & Ferrari, A. 2008, *A&A*, 488, 795
- Sanders, R. H. 1983, *ApJ*, 266, 73
- Takeuchi, S., Ohsuga, K., & Mineshige, S. 2013, *PASJ*, 65, 88
- Takeuchi, S., Ohsuga, K., & Mineshige, S. 2014, *PASJ*, 66, 48
- Taylor, G. 1950, *Royal Society of London Proceedings Series A*, 201, 192
- Toma, K., Komissarov, S. S., & Porth, O. 2017, *arXiv:1705.10425*
- Turland, B. D., & Scheuer, P. A. G. 1976, *MNRAS*, 176, 421
- Urpín, V. 2002, *A&A*, 385, 14
- Warren, D. C., & Blondin, J. M. 2013, *MNRAS*, 429, 3099
- Wongwathanarat, A., Müller, E., & Janka, H.-T. 2015, *A&A*, 577, A48
- Zenitani, S., Hesse, M., & Klimas, A. 2010, *ApJ*, 712, 951